NANO LETTERS

pubs.acs.org/NanoLett Letter

Hyperbolic Cooper-Pair Polaritons in Planar Graphene/Cuprate Plasmonic Cavities

Michael E. Berkowitz,[▽] Brian S. Y. Kim,[▽] Guangxin Ni, Alexander S. McLeod, Chiu Fan Bowen Lo, Zhiyuan Sun, Genda Gu, Kenji Watanabe, Takashi Taniguchi, Andrew J. Millis, James C. Hone, Michael M. Fogler, Richard D. Averitt, and D. N. Basov*

Cite This: *Nano Lett.* 2021, 21, 308−316 Read Online

ACCESS | Metrics & More | Article Recommendations | Supporting Information

ABSTRACT: Hyperbolic Cooper-pair polaritons (HCP) in cuprate superconductors are of fundamental interest due to their potential for providing insights into the nature of unconventional superconductivity. Here, we critically assess an experimental approach using near-field imaging to probe HCP in $Bi_2Sr_2CaCu_2O_{8+x}$ (Bi-2212) in the presence of graphene surface plasmon polaritons (SPP). Our simulations show that inherently weak HCP features in the near-field can be strongly enhanced when coupled to graphene SPP in layered graphene/hexagonal boron nitride (hBN)/Bi-2212 heterostructures. This enhancement arises from our multilayered structures effectively acting as plasmonic cavities capable of altering collective modes of a layered superconductor by modifying its electromagnetic environment. The degree of enhancement can be selectively controlled by tuning the insulating spacer thickness with atomic precision. Finally, we verify the expected renormalization of room-temperature graphene SPP using near-field infrared imaging. Our modeling, augmented with data, attests to the validity of our approach for probing HCP modes in cuprate superconductors.

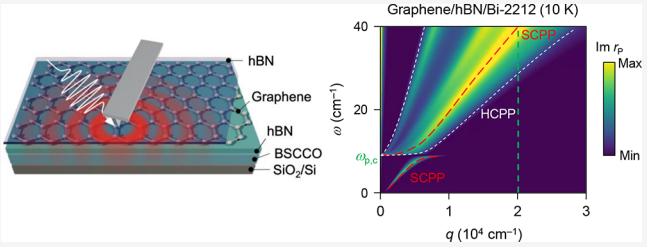

KEYWORDS: *Cuprate superconductors, graphene, hyperbolic Cooper-pair polaritons, plasmonic cavities, van der Waals heterostructures, scattering-type scanning near-field microscopy*

Hyperbolic energy-momentum (ω,q) dispersion relations arise in uniaxial materials when the dielectric permittivity exhibits opposite signs along different directions, leading to a hyperbolic isofrequency surface in k-space.[1] This unusual optical behavior offers exciting opportunities for fundamental studies and applications, including spontaneous emission enhancement, negative refraction, and enhanced superlensing effects.[1] In particular, cuprate high-temperature superconductors can be classified as natural hyperbolic materials (NHM)[2,3] with hyperbolicity arising from the strong electronic anisotropy dictated by their layered crystal structure.[4−10] The rich electrodynamics associated with the hyperbolic response in the cuprates and specifically hyperbolic Cooper-pair polariton (HCP) modes in these materials remain underexplored. Optical studies of HCP modes are of fundamental interest; HCP modes not only allow for the precise extraction of optical response functions but also shed light on the nature of unconventional superconductivity.[11] Furthermore, the connection between the hyperbolic modes and attractive electron−electron interactions in the cuprates could provide useful insights into further enhancing T_c in nanoengineered metamaterial superconductors.[12]

The cuprate superconductor $Bi_2Sr_2CaCu_2O_{8+x}$ (Bi-2212) features weak van der Waals (vdW) bonding between neighboring BiO planes along the interlayer c-axis direction (Figure 1a). The ability to exfoliate Bi-2212 allows for the creation of vdW heterostructures with novel optical properties, where HCP can be strongly coupled and hybridized with other polaritonic modes of proximal layers.[9] However, detailed experimental and theoretical studies of Bi-2212 HCP modes are yet to be systematically pursued. One major challenge arises from the spectral location of the HCP modes, which lie in the "high q" regime with $q > \omega/c$, where ω is the excitation frequency and c is the speed of light in vacuum. Probing these high q modes often involves complex momentum-matching techniques using nanofabrication,[13] which is especially challenging for Bi-2212 considering its air sensitivity.[14]

In this work, we critically assess an experimental approach utilizing scattering-type scanning near-field optical microscopy (s-SNOM) to probe HCP modes in cuprates. We first survey the emergence of hyperbolic dispersion relation in Bi-2212 using the experimentally measured dielectric function available

Received: September 10, 2020
Revised: December 8, 2020
Published: December 15, 2020

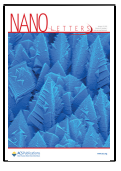

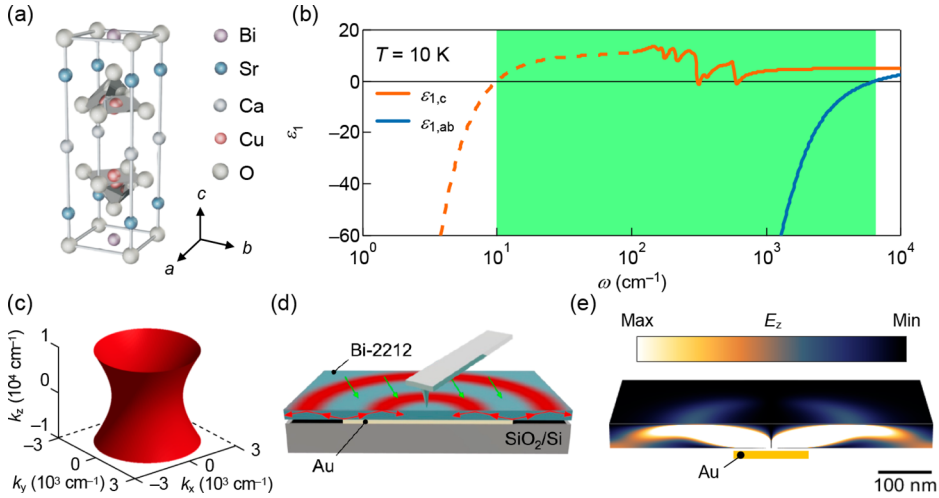

Figure 1. (a) The half-unit-cell of Bi-2212 crystal structure containing two CuO_2 planes. (b) The real part of Bi-2212 dielectric function in the *ab*-plane $\varepsilon_{1,ab}$ (blue solid line) and the *c*-axis $\varepsilon_{1,c}$ (orange solid line) from THz through IR frequencies at T = 10 K. The orange dashed line is $\varepsilon_{1,c}$ calculated based on the two-fluid model (see text). (c) Isofrequency surface of Bi-2212 at ω = 905 cm^{-1} displaying a hyperbolic dispersion relation: $\varepsilon_{1,ab} < 0$, $\varepsilon_{1,c} > 0$. (d) Schematic of the hyperbolic ray propagation in Bi-2212 probed using scattering-type scanning near-field optical microscopy (s-SNOM). The hyperbolic Cooper-pair polariton (HCP) mode is launched from a lithographically defined Au disk edge underneath the Bi-2212. (e) The simulated *z*-component of the electric field for the hyperbolic ray launched at the disk edge at ω = 905 cm^{-1} and at T = 10 K. Note that the HCP propagation is significantly damped and therefore does not produce an observable s-SNOM signal.

for the *ab*-plane and the *c*-axis. On the basis of this observation, we model the s-SNOM observables attributable to HCP modes for bare Bi-2212 layers. We find that HCP features are inherently weak and may be difficult to detect in s-SNOM experiments. We present the design of a layered graphene/hexagonal boron nitride (hBN)/Bi-2212 heterostructure that serves as a platform for enhancing HCP features, arising from strong coupling between graphene surface plasmon polariton (SPP) modes and Bi-2212 HCP modes. The hybridization of SPP/HCP modes is clearly reflected in our modeling as an avoided crossing of the SPP at the *c*-axis interbilayer Josephson plasma resonance (JPR) frequency. Moreover, we find that the degree of hybridization of the SPP with each HCP branch can be selectively controlled by tuning the thickness of hBN spacers with atomic precision. Naturally, the hybridization is maximized whenever the SPP mode maximally overlaps with certain HCP branches. The coupling between the graphene SPP mode and Bi-2212 is further reflected in our simulations by the renormalization of the graphene SPP mode dispersion. The net effect is that collective modes of Bi-2212 superconductor are modified when hybridized with graphene plasmons. Therefore, our heterostructures act as plasmonic cavities[10,15] enabling exquisite control of the electromagnetic environment of a layered superconductor. To verify the general feasibility of our proposal, we perform near-field imaging of the mid-IR SPP mode in the graphene/hBN/Bi-2212 heterostructure at room temperature. The key finding is that the graphene SPP mode is renormalized as expected, confirming the strong coupling between graphene and Bi-2212. This strong coupling would serve as an essential ingredient for the hybridization of graphene SPP with Bi-2212 HCP modes in low temperatures. Therefore, our results provide a robust platform for using s-SNOM to probe HCP modes in cuprate superconductors over a wide spectral range.

Bi-2212 is an anisotropic layered superconductor (T_c = 91 K) in which the normal state optical conductivity profile of the *ab*-plane is metallic due to the presence of CuO_2 planes, while that of the *c*-axis is nearly insulating (Figure 1a).[11] This strong anisotropy in Bi-2212 results in a dielectric function with a hyperbolic dispersion relation over a large spectral region in which $\varepsilon_{1,ab}\varepsilon_{1,c} < 0$, where $\varepsilon_{1,ab}$ and $\varepsilon_{1,c}$ are the real part of Bi-2212 dielectric function in the *ab*-plane and the *c*-axis, respectively.[16] To obtain further insight into the hyperbolic electrodynamic response in Bi-2212, we survey the *ab*-plane and *c*-axis dielectric functions from infrared (IR) to terahertz (THz) frequencies (down to 100 cm^{-1}) using data from refs 17 and 18 at T = 10 K. For frequencies lower than 100 cm^{-1}, we extrapolate these existing data using the two-fluid model (see Supporting Information for detailed calculations). We constrained the input parameters to ensure that the low-temperature dielectric function self-consistently crosses zero at the *c*-axis interbilayer JPR frequency $\omega_{p,c}$ (~10 cm^{-1} for optimally doped Bi-2212[19,20]).

Figure 1b shows the dielectric function of Bi-2212 down to 1 cm^{-1} at T = 10 K. The key observation is that the real part of both the *ab*-plane and *c*-axis dielectric functions crosses zero at their respective plasma frequencies, which occurs due to the dielectric constant diverging to $-\infty$ in the low-frequency limit. As a result, $\varepsilon_{1,ab}$ and $\varepsilon_{1,c}$ have opposite signs in the spectral region bounded by the plasma frequencies in the *ab*-plane and the *c*-axis, $\omega_{p,c} < \omega < \omega_{p,ab}$ (green shaded area in Figure 1b). We calculate the associated isofrequency surface of Bi-2212 within this hyperbolic spectral region (specifically, at ω = 905 cm^{-1}) which exhibits, as expected, hyperbolic dispersion (Figure 1c). Therefore, our analysis predicts that Bi-2212 supports propagating hyperbolic waveguide modes accompanied by a collection of HCP branches across a wide spectral range of ~10−8000 cm^{-1}.[6,21] We note that the precise value of $\omega_{p,c}$ is of particular importance because the HCP branches are immediately quenched for $\omega < \omega_{p,c}$. One may therefore also use Bi-2212 hyperbolic phenomena as an optical probe to study the interlayer Josephson effects.[22,23]

s-SNOM can couple electromagnetic fields with high intensity in the subdiffraction limit[24−28] and is therefore an ideal probe for imaging various high-q polariton modes in layered materials.[29,30] We theoretically analyze the feasibility of

https://dx.doi.org/10.1021/acs.nanolett.0c03684
Nano Lett. 2021, 21, 308−316

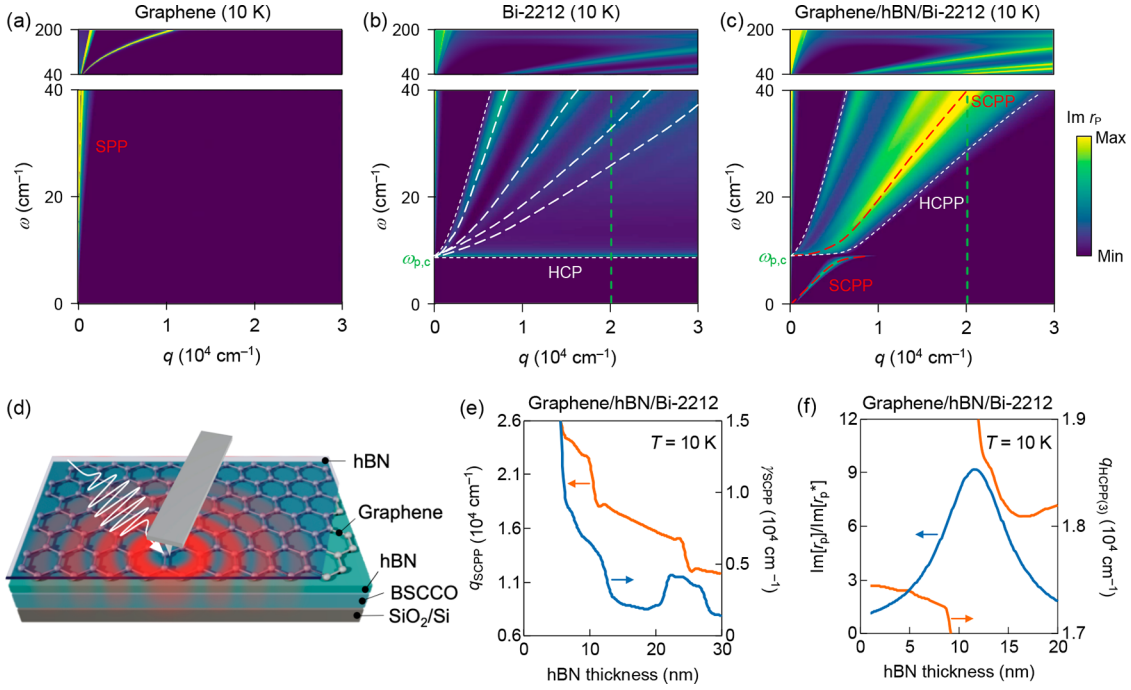

Figure 2. Mode hybridization in graphene/hBN/Bi-2212 plasmonic cavities. Imaginary part of the p-polarized reflection coefficient (Im[r_p]) of (a) graphene, (b) Bi-21212, and (c) the layered graphene/hBN/Bi-2212 heterostructure with 16 nm hBN at T = 10 K. $\omega_{p,c}$ is the c-axis interbilayer Josephson plasma resonance frequency. The vertical green dashed line in (b,c) marks the in-plane momentum at which the s-SNOM tip−sample coupling is maximized. The hybridization of the SPP and HCP modes is indicated by the avoided crossing at $\omega = \omega_{p,c}$, resulting in the appearance of the SCPP branch below $\omega = \omega_{p,c}$ while both SCPP and HCPP branches appear above $\omega_{p,c}$. The white dashed lines in (b,c) are guides to the eye for HCP and HCPP modes, respectively. The red dashed line in (c) is the guide to the eye for the SCPP mode. (d) Schematic of the proposed s-SNOM experiment for imaging Bi-2212 HCP in the layered graphene/hBN/Bi-2212 heterostructure. The collective modes launched by the AFM tip extend into the Bi-2212 layer, emphasizing the hybridization of SPP in graphene with HCP in Bi-2212, each forming SCPP and HCPP, respectively. (e) Interlayer hBN thickness dependence of SCPP wavevector q_{SCPP} (solid orange line) and scattering rate γ_{SCPP} (solid blue line) at ω = 33 cm^{-1} and at T = 10 K. As the hBN thickness increases, both q_{SCPP} and γ_{SCPP} asymptotically approach the limits of the hBN/graphene/hBN heterostructure. (f) Interlayer hBN thickness dependence of Im[r_p] of the third-order HCPP (HCPP$^{(3)}$) mode normalized to that of HCP$^{(3)}$ mode (Im[r_p*]) (solid blue line), and the HCPP$^{(3)}$ mode wavevector $q_{HCPP(3)}$ (solid orange line). Both line profiles are taken at ω = 33 cm^{-1} and at T = 10 K. The HCPP mode strength enhancement via interaction with graphene SCPP is maximized when the HCPP and SCPP branches maximally overlap at an intermediate interlayer hBN thickness.

imaging observables attributable to HCP for Bi-2212 layers in s-SNOM measurements. Specifically, we simulate the propagation of hyperbolic waveguide modes launched at the edge of the gold disk placed underneath Bi-2212 at T = 10 K (Figure 1d; see Supporting Information for simulation details). Placing metallic antennas beneath NHMs has proven effective for resonantly exciting and imaging the propagation of hyperbolic waveguide modes in s-SNOM measurements.[30−32] However, our simulations show that the HCP propagation is significantly damped and unlikely to produce an observable s-SNOM signal for any Bi-2212 microcrystals with thicknesses that can support multiple HCP branches ($d_{Bi\text{-}2212} \geq$ 10 nm; Figure 1e). The major source of this weak near-field response can be attributed to losses from residual quasiparticle excitations. Furthermore, the extreme anisotropy of Bi-2212 ($|\varepsilon_{1,ab}| \gg |\varepsilon_{1,c}|$) produces HCP rays for which $k_z \gg q$, resulting in (1) charge density oscillations which are out of phase between different CuO_2 planes and (2) ray propagation nearly parallel to the ab-plane, resulting in a longer propagation length (and thus larger loss) before reflection at Bi-2212 boundaries.[30] We therefore conclude that observing HCP modes launched in bare Bi-2212 flakes would be fundamentally challenging in s-SNOM measurements.

To enhance the near-field signatures of HCP modes, we design a layered vdW plasmonic cavity composed of graphene and Bi-2212 separated by an hBN layer. In general, graphene exhibits tunable SPP modes from IR to THz frequencies,[29,33−35] which readily hybridize with collective modes in natural hyperbolic compounds. For example, graphene SPP modes hybridize with hBN hyperbolic phonon−polariton modes, forming highly confined hyperbolic plasmon−phonon polaritons.[36,37,38] We leverage the strong coupling capabilities of graphene SPP modes to enhance the low-lying Bi-2212 HCP modes using the graphene/hBN/Bi-2212 heterostructure shown in Figure 2d. Importantly, in our plasmonic cavities a variable interlayer hBN thickness is used to tune the coupling between the graphene SPP and the Bi-2212 HCP with atomic precision.

We quantitatively determine the SPP/HCP coupling by simulating the p-polarized reflection coefficient (r_p) of the graphene/hBN/Bi-2212 heterostructure using the transfer matrix method.[39] Here, we define r_p as the ratio of the complex amplitude of the reflected wave to that of the incident wave. This approach clearly visualizes the dispersion and coupling of the entire collective mode spectrum present in the system. As inputs, we use the Bi-2212 dielectric response described above and the dielectric functions from ref 40 for graphene and ref 41 for hBN. We use the local approximation where $\varepsilon(\omega,q) = \varepsilon(\omega,0)$, which is valid for the following limits (that are satisfied for our heterostructure):[40] (1) $q \ll k_F$ and

https://dx.doi.org/10.1021/acs.nanolett.0c03684
Nano Lett. 2021, 21, 308−316

(2) $\omega/q \gg v_F$, where k_F is the Fermi wavevector, and v_F is the Fermi velocity. Under our local approximation, possible Higgs amplitude and Bardasis−Schrieffer (BaSh) collective modes are neglected since they respond to electric field only at nonzero q.[21] Note that Bi-2212 c-axis electrodynamics possess nonlinear characteristics prompted by the Josephson physics. For example, this nonlinearity can be amplified in the vicinity of the JPR frequencies, leading to short, intense THz pulses[42] which could potentially interact nonlinearly with THz graphene plasmons.[43] Here, we focus on the linear response regime as s-SNOM experiments relevant for our studies are typically performed in the weak-field limit. We further note that Bi-2212 supports other plasma modes, including transverse plasma mode (TPM) in the IR regime.[11] This latter feature arises from the presence of a CuO_2 bilayer in Bi-2212.[11,44,45] We find that the TPM is negligible in our r_p calculations due to the low interbilayer conductivity of Bi-2212[46] which leads to a small spectral weight associated with TPM[47] (see Supporting Information for detailed simulations).

We tune the interlayer hBN thickness in our simulations based on the following three considerations relevant for s-SNOM measurements (see Supporting Information for detailed optimizations). First, we minimize damping to maximize the number of polariton fringes potentially visible in near-field imaging experiments. We characterize the damping from the full width at half-maximum of the mode visualized in the $\mathrm{Im}[r_p]$ plot. Polaritonic damping in our heterostructure can be expressed as the sum of scattering rate contributions from loss channels intrinsic in graphene (γ_{gr}) (see ref 29 for details) and in Bi-2212 ($\gamma_{Bi\text{-}2212}$). We tune the influence of $\gamma_{Bi\text{-}2212}$ by changing the distance between the graphene and Bi-2212. Second, we tune the momentum of the collective modes present in the heterostructure as close as possible to the in-plane momentum of s-SNOM tip, $q^* \sim 1/a$, where a is the tip radius (a = 20 nm at IR frequencies,[26] 500 nm at THz frequencies[48]). Third, we maximize the $\mathrm{Im}[r_p]$ intensity of the HCP modes by aligning one of the HCP modes of Bi-2212 and the SPP mode of graphene such that they maximally overlap in the dispersion diagram. We note that the interlayer hBN in our heterostructure naturally enables Bi-2212 to gate graphene to support tunable SPP modes. This sets the practical limit of hBN thickness to be on the order of several nanometers in our studies, below which tunneling current would dominate and controlling the carrier density in graphene would become challenging. Nonetheless, one interesting limit is the graphene in direct contact to Bi-2212 with no interlayer hBN. In this limit, some degree of interfacial charge transfer could occur[49] and give rise to novel plasmonic features associated with interface-induced phenomena specific to a metal-superconductor interface, including Andreev reflection[50] and proximity effect.[51]

Figure 2a,b shows our r_p simulations for individual graphene and Bi-2212 layers at THz frequencies revealing their characteristic collective mode spectra. At these frequencies, the graphene SPP modes are located very close to the light line as expected. In Bi-2212, multiple HCP branches emerge above $\omega_{p,c}$, where the separation between the HCP branches is dictated by the thickness of the slab (see Supporting Information for detailed simulations). Another important observation is that at ω = 33 cm^{-1}, the third-order HCP mode ($HCP^{(3)}$) q coincides with q^*, providing an opportunity to study the evolution of the $HCP^{(3)}$ mode upon hybridization with graphene SPP modes in our graphene/hBN/Bi-2212 heterostructure.

Figure 2c shows the rich electrodynamic response of altered collective modes that emerge in our graphene/hBN/Bi-2212 plasmonic cavities. This includes surface Cooper-pair plasmon polariton (SCPP) modes and hyperbolic Cooper-pair plasmon polariton (HCPP) modes, which arise from mixing of SPP and HCP modes, while each retaining some degree of their original character. The hybridization between SPP/HCP modes is reflected by the avoided crossing of SCPP modes at $\omega_{p,c}$.[52] Further, the quenching of the HCPP modes below $\omega_{p,c}$ indicates that they retain the hyperbolic character of the HCP modes. To verify whether SCPP mode retains its surface character, we studied the dependence of the SCPP and HCPP mode scattering rates on the intrinsic graphene scattering rate γ_{gr} (Figure S10). Our simulation shows that the SCPP mode scattering rate linearly correlates with γ_{gr}. In contrast, the HCPP mode scattering rate is only affected by changes in γ_{gr} when the HCPP branch is relatively close to the SCPP branch, illustrating that SCPP modes retain their surface character. More interestingly, this indicates that even HCPP exhibits a surface character when the HCPP branch is in proximity to the SCPP branch and the two modes become strongly hybridized.

Our plasmonic cavity provides an exciting opportunity to study the mixing of the two modes by screening the SPP mode away from the light line and toward the HCP branches where they hybridize and become SCPP and HCPP modes. This renormalization of the SPP dispersion is produced by the formation of image charges in Bi-2212 which screen the long-range Coulomb interaction in graphene. The resultant overlap of SCPP and HCPP modes allows us to selectively control the hybridization by tuning the interlayer hBN thickness with atomic precision. Figure 2e shows the evolution of the SCPP mode wavevector q_{SCPP} and scattering rate γ_{SCPP} as a function of interlayer hBN thickness. The general trend is that both q_{SCPP} and γ_{SCPP} decrease with increasing hBN thickness as the effect of screening and coupling to loss channels present in Bi-2212 are reduced, respectively. We note that whenever SCPP modes are in proximity to HCPP modes, there is a nonmonotonic evolution of q_{SCPP} resulting from the coupling between the two modes. Specifically, q_{SCPP} abruptly decreases as the SCPP mode maximally overlaps with the HCPP modes (occurring at ∼24 and ∼12 nm for second order HCPP ($HCPP^{(2)}$) and third order HCPP ($HCPP^{(3)}$) modes, respectively). In contrast, we find considerable peaks in q_{SCPP} (repulsion of SCPP modes from HCPP modes) whenever the SCPP mode only partially overlaps with the HCPP modes, indicative of strong coupling with the HCPP modes.

We next focus on the $HCPP^{(3)}$ mode as its wavevector $q_{HCPP(3)}$ coincides with the tip momentum q^* for our frequencies of interest as discussed above. Figure 2f shows the evolution of $q_{HCPP(3)}$ at ω = 33 cm^{-1}, along with its mode intensity enhancement factor as described by the ratio of the maximum r_p with respect to that for the bare Bi-2212 flake. We find that the $HCPP^{(3)}$ mode intensity is enhanced by nearly an order of magnitude when the SCPP and HCPP modes overlap. Furthermore, $q_{HCPP(3)}$ diverges as SCPP branch approaches the $HCPP^{(3)}$ mode branch. This verifies that the observed repulsion of the mode wavevector is a mutual effect between the SCPP and HCPP modes due to strong coupling.

We emphasize that the interlayer hBN thickness is the key parameter in designing our heterostructure, considering that the coupling between the SCPP and HCPP modes naturally

https://dx.doi.org/10.1021/acs.nanolett.0c03684
Nano Lett. 2021, 21, 308−316

fades away at larger interlayer hBN thickness. Figure 3 shows the evolution of coupling between SCPP and HCPP modes at

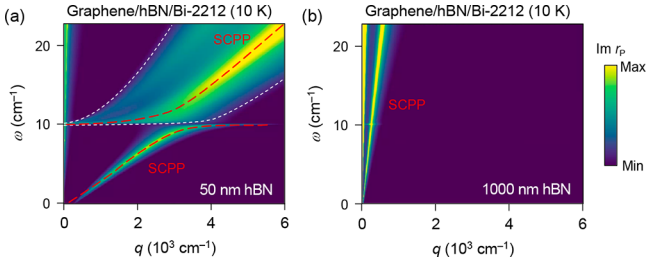

Figure 3. Im[r_p] of the layered graphene/hBN/Bi-2212 heterostructure at T = 10 K with interlayer hBN of thickness (a) 50 nm and (b) 1000 nm. The white and red dashed lines in (a) are guides to the eye for HCPP and SCPP modes, respectively. The avoided crossing indicating coupling between the SCPP and HCPP modes is clearly visible for (a) 50 nm hBN but becomes progressively weaker as the layer thickness increases and is unnoticeable for (b) 1000 nm hBN (see Supporting Information for more details on mode coupling and the avoided crossing).

two representative interlayer hBN thicknesses. Notably, the avoided crossing of SCPP modes is still present for 50 nm thick hBN (Figure 3a). However, as the thickness of the interlayer hBN increases, the avoided crossing gradually weakens and becomes completely negligible for 1000 nm thick hBN (Figure 3b). The collective mode dispersion for the graphene/hBN/Bi-2212 heterostructure shown in Figure 2c is designed using optimal parameters chosen based on the simulation presented above, which consist of graphene Fermi energy E_F of ∼370 meV, 16 nm interlayer hBN, and 50 nm Bi-2212. This parameter set optimizes the aforementioned metrics for s-SNOM imaging of hybridized HCPP modes (tuned screening, minimal damping, and maximal enhancement of the HCPP$^{(3)}$ mode).[35] Our modeling therefore demonstrates strong coupling of the SPP and HCP modes in our plasmonic cavity, enabling near-field imaging a viable probe for examining HCPP at THz frequencies.

To verify our approach for probing plasmonic features and associated HCP modes in Bi-2212, we image mid-IR SPP modes in the layered graphene/hBN/Bi-2212 heterostructure at room temperature. Using the simulation results discussed above, we assemble the heterostructure with 16 nm thick interlayer hBN and 50 nm thick Bi-2212 (Figure 4a). The device is assembled using a polymer-free dry-transfer process[53] in a glovebox filled with inert gas to minimize Bi-2212 degradation (see Supporting Information). Figure 4b shows the transport properties of a ∼50 nm Bi-2212 flake prepared using the same assembly scheme but without graphene or hBN layers on top. The extracted T_c is near the bulk value of ∼91 K, indicating that our Bi-2212 flakes retain bulk superconducting properties. Figure 4c shows the two-probe graphene sheet resistance $R_{2\ pt}$ as a function of Bi-2212 gate voltage V_g at 300 K, where clear resistance peak corresponding to the charge neutrality point is observed. This indicates that Bi-2212 can successfully dope graphene. Infrared near-field imaging is performed using laser excitation at ω = 905 cm^{-1} while gating graphene to E_F ∼ 370 meV (see Supporting Information for measurement details). Our imaging reveals clear plasmonic interference fringes, resulting from interference between SPP modes launched from the AFM tip and their reflection off of

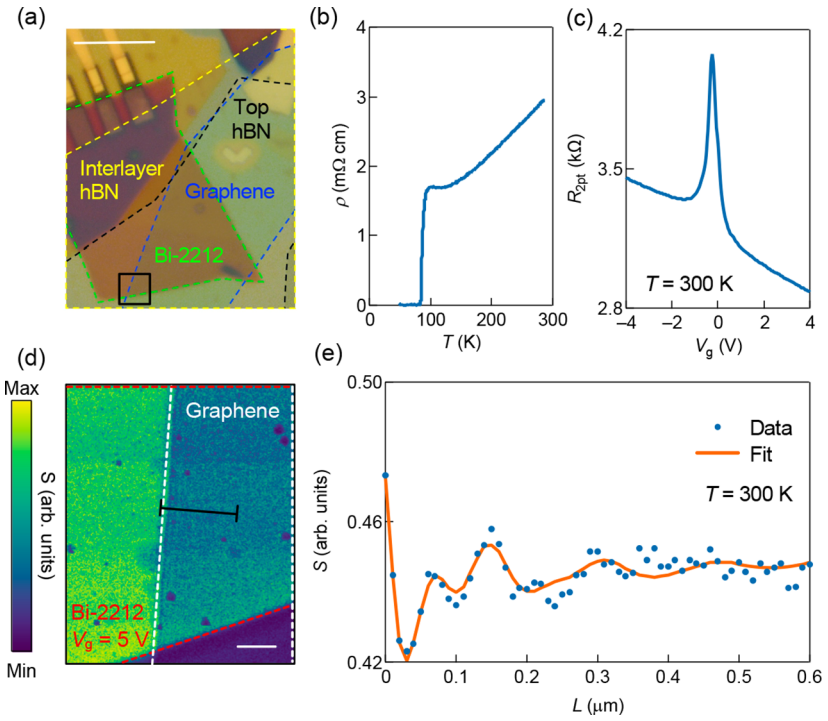

Figure 4. (a) Optical image of the layered graphene/hBN/Bi-2212 heterostructure. Scale bar: 10 μm. The black square represents the scanned area of the near-field imaging experiments shown in panel (d). The AFM tip serves as an effective plasmonic launcher while the graphene edge serves as a plasmonic reflector. Scale bar: 10 μm. (b) Resistivity of ∼50 nm thick Bi-2212 layer as a function of T. (c) Two-probe graphene resistance $R_{2\ pt}$ as a function of Bi-2212 gate voltage V_g at T = 300 K. (d) Experimental near-field image $S(r,\omega)$ acquired at V_g = 5 V demodulated at the fifth harmonic (ω = 905 cm^{-1} and T = 300 K). The black line represents the location of the line profiles in panel (e). Scale bar: 500 nm. (e) A line profile of $S(r,\omega)$ (blue solid circles) showing the interference fringes produced by the graphene SPP. The orange solid line is the fit (see text).

https://dx.doi.org/10.1021/acs.nanolett.0c03684
Nano Lett. 2021, 21, 308−316

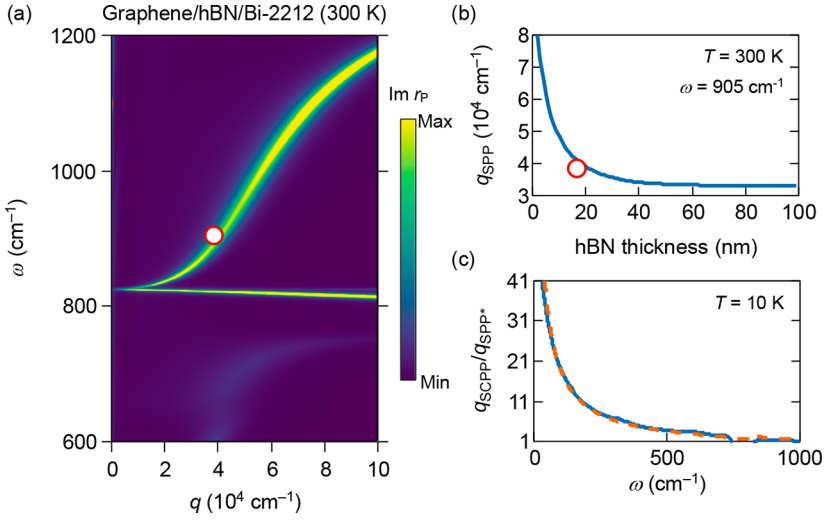

Figure 5. (a) Im[r_p] of the layered graphene/hBN/Bi-2212 heterostructure at T = 300 K in the IR regime. (b) SPP wavevector q_{SPP} as a function of the interlayer hBN thickness extracted from r_p calculations at ω = 905 cm^{-1} and at T = 300 K. The red open circle in (a,b) is the experimental data. (c) Graphene SPP renormalization factor q_{SCPP}/q_{SPP*} as a function of ω at T = 10 K. q_{SPP*} is the bare SPP wavevector in graphene/hBN heterostructure without Bi-2212. The solid blue line is the simulated data and the solid orange line is the fit based on the theoretical model presented in the main text. The data show excellent agreement with the fit.

the graphene edge (Figure 4d).[40] We fit the observed near-field fringes using a linear combination of a damped harmonic oscillator and a Hankel function to extract a plasmon wavevector q_{SPP} of 3.81 × 10^5 cm^{-1} and the SPP quality factor Q_{SPP} (= Re[q_{SPP}]/Im[q_{SPP}]) of 8.14.

Figure 5a shows our r_p simulations for the graphene/hBN/Bi2212 heterostructure in the IR regime. We find that q_{SPP} and Q_{SPP} extracted from our imaging experiment agree well with the simulated values of 4.16 × 10^5 cm^{-1} and 7.56, respectively. This overall consistency shows that our analysis reliably captures the gross features of electrodynamics of our graphene/hBN/Bi-2212 heterostructure. In our simulations, we assume that graphene has mobility limited by the electron−phonon scattering rate at room temperature (γ_{gr} of ∼10 cm^{-1} at THz frequencies and ∼15 cm^{-1} at IR frequencies).[29] Our experimental result therefore indicates that our choice of 16 nm interlayer hBN effectively screens and minimizes any extrinsic source of scattering of the electrons in graphene, including possible impurities from the underlying Bi-2212.[54] More importantly, we confirm that the extracted q_{SPP} is renormalized as expected, verifying the strong coupling between graphene and Bi-2212. Furthermore, the screening of the SPP dispersion can be precisely controlled by tuning the interlayer hBN thickness (Figure 5b). It is this direct tunability of screening which enables us to selectively control the coupling between SPP and certain HCP branches in the THz regime by varying interlayer hBN thickness, as discussed above.

We can quantify the screening of SPP mode by observing the necessary condition for producing graphene SCPP

$$1 + \frac{2\pi i q}{\omega \epsilon(\omega, q)}\sigma(\omega) = 0 \quad (1)$$

where σ is the optical conductivity of graphene and $\epsilon(\omega, q)$ is the effective screening from the environment surrounding graphene. While ϵ is $\sim\sqrt{\epsilon^x_{hBN}\epsilon^z_{hBN}}$ in the limit of thick hBN, it is enhanced to $\sim\sqrt{\epsilon^x_{hBN}\epsilon^z_{hBN}}/(qd)$ by the superconducting Bi-2212 slab when $\lambda \gg d$, where d is the interlayer hBN thickness and λ is the plasmon wavelength.[35] This relative increase in the screening induces a commensurate increase in q by a factor of $\sim\sqrt{\lambda/d}$ to maintain the self-oscillation condition shown in eq 1.[35,55] These changes produce a self-consistent renormalization of SPP dispersion toward higher q in our simulations. This can be verified from the screening ratio of q_{SCPP}/q_{SPP*} scaling as $\sim\sqrt{\lambda/d}$, where q_{SPP*} is the bare SPP wavevector in graphene/hBN heterostructure without Bi-2212 (Figure 5c). We emphasize that the renormalization of the plasmonic dispersion is most pronounced in the THz regime where Bi-2212 HCP modes reside (Figure 5c). Because strong coupling is confirmed by our experiments, this coupling is guaranteed to persist below T_c and will serve as an essential ingredient for the hybridization of graphene SPP with Bi-2212 HCP modes.

In conclusion, we have demonstrated that the layered graphene/hBN/Bi-2212 heterostructure can serve as a robust cavity platform for studying Bi-2212 HCP using s-SNOM. Our modeling shows that strong coupling between graphene SPP and Bi-2212 HCP results in the hybridized HCPP observable in s-SNOM experiments. We have also probed the expected renormalization of mid-IR graphene SPP in the proposed heterostructure, demonstrating the feasibility of our proposal. Considering the advances in cryogenic near-field imaging techniques,[29,56] we predict that HCPP modes are experimentally accessible down to JPR frequencies at THz frequencies and at low temperatures. The techniques outlined in this paper pave the way for further investigation of collective modes and cavity electrodynamics of unconventional superconductors using cryogenic s-SNOM.[57,58]

■ ASSOCIATED CONTENT

Supporting Information

The Supporting Information is available free of charge at https://pubs.acs.org/doi/10.1021/acs.nanolett.0c03684.

Detailed description of the device fabrication, electrical characterization, near-field measurements, hyperbolic ray propagation, transfer matrix formalism, Bi-2212 dielectric function in the low-frequency limit, and supplementary simulation profiles (PDF)

https://dx.doi.org/10.1021/acs.nanolett.0c03684
Nano Lett. 2021, 21, 308−316

AUTHOR INFORMATION

Corresponding Author

D. N. Basov − *Department of Physics, Columbia University, New York 10027, United States*; Email: db3056@columbia.edu

Authors

Michael E. Berkowitz − *Department of Physics, Columbia University, New York 10027, United States*; orcid.org/0000-0001-5962-2857

Brian S. Y. Kim − *Department of Physics and Department of Mechanical Engineering, Columbia University, New York 10027, United States*

Guangxin Ni − *Department of Physics, Columbia University, New York 10027, United States*

Alexander S. McLeod − *Department of Physics, Columbia University, New York 10027, United States*

Chiu Fan Bowen Lo − *Department of Physics, Columbia University, New York 10027, United States*

Zhiyuan Sun − *Department of Physics, Columbia University, New York 10027, United States*

Genda Gu − *Condensed Matter Physics and Material Science Department, Brookhaven National Laboratory, Upton, New York 11973, United States*

Kenji Watanabe − *Research Center for Functional Materials, National Institute of Material Science, Ibaraki 305-0044, Japan*; orcid.org/0000-0003-3701-8119

Takashi Taniguchi − *International Center for Materials Nanoarchitectonics, National Institute of Material Science, Ibaraki 305-0044, Japan*; orcid.org/0000-0002-1467-3105

Andrew J. Millis − *Department of Physics, Columbia University, New York 10027, United States*

James C. Hone − *Department of Mechanical Engineering, Columbia University, New York 10027, United States*

Michael M. Fogler − *Department of Physics, University of California San Diego, La Jolla, California 92093, United States*

Richard D. Averitt − *Department of Physics, University of California San Diego, La Jolla, California 92093, United States*

Complete contact information is available at: https://pubs.acs.org/10.1021/acs.nanolett.0c03684

Author Contributions

$^{\nabla}$M.E.B. and B.S.Y.K. contributed equally to this work.

Notes

The authors declare no competing financial interest.

ACKNOWLEDGMENTS

Research on hybrid heterostructures was supported by the Center on Precision-Assembled Quantum Materials, funded through the U.S. National Science Foundation (NSF) Materials Research Science and Engineering Centers (award no. DMR-2011738). D.N.B. is Moore Investigator in Quantum Materials EPIQS #9455 and the Vannevar Bush Faculty Fellow ONR-VB: N00014-19-1-2630. M.M.F. acknowledges support from ONR-N000141812722. K.W. and T.T. acknowledge support from the Elemental Strategy Initiative conducted by the MEXT, Japan, Grant JPMXP0112101001, JSPS KAKENHI Grant JP20H00354, and the CREST(JPMJCR15F3), JST. The work at BNL was supported by the US Department of Energy, office of Basic Energy Sciences, contract no. DOE-sc0012704. R.D.A. acknowledges support from ARO Award No. W911NF-16-1-0361.

ABBREVIATIONS

HCP, hyperbolic Cooper-pair polariton; Bi-2212, $Bi_2Sr_2CaCu_2O_{8+x}$; hBN, hexagonal boron nitride; SPP, surface plasmon polariton; SCPP, surface Cooper-pair plasmon polariton; HCPP, hyperbolic Cooper-pair plasmon polariton; vdW, van der Waals; s-SNOM, scattering-type scanning near-field optical microscopy; JPR, Josephson plasma resonance; NHM, natural hyperbolic materials; BaSh, Bardasis-Schrieffer; TPM, transverse plasma mode; IR,, infrared; THz, terahertz

REFERENCES

(1) Poddubny, A.; Iorsh, I.; Belov, P.; Kivshar, Y. Hyperbolic Metamaterials. *Nat. Photonics* **2013**, *7*, 948−957.

(2) Korzeb, K.; Gajc, M.; Pawlak, D. A. Compendium of natural hyperbolic materials. *Opt. Express* **2015**, *23*, 25406−25424.

(3) Lee, Y. U.; Gaudin, O. P. M.; Lee, K.; Choi, E.; Placide, V.; Takaishi, K.; Muto, T.; Andre, P.; Muranaka, A.; Uchiyama, M.; Mathevet, F.; Aoyama, T.; Wu, J.; D'Aleo, A.; Ribierre, J.-C. Organic monolithic natural hyperbolic material. *ACS Photonics* **2019**, *6*, 1681−1689.

(4) Romanowsky, M.; Capasso, F. Orientation-dependent Casimir force arising from highly anisotropic crystals: Application to $Bi_2Sr_2CaCu_2O_{8+\delta}$. *Phys. Rev. A* **2008**, *78*, 042110−042115.

(5) Sun, J.; Litchinitser, N. M.; Zhou, J. Indefinite by nature: From ultraviolet to terahertz. *ACS Photonics* **2014**, *1*, 293−303.

(6) Stinson, H. T.; Wu, J. S.; Jiang, B. Y.; Fei, Z.; Rodin, A. S.; Chapler, B. C.; McLeod, A. S.; Castro Neto, A.; Lee, Y. S.; Fogler, M. M.; Basov, D. N. Infrared nanospectroscopy and imaging of collective superfluid excitations in anisotropic superconductors. *Phys. Rev. B* **2014**, *90*, 014502−014512.

(7) Smolyaninov, I. I. Quantum topological transition in hyperbolicmetamaterials based on high T_c superconductors. *J. Phys.: Condens. Matter* **2014**, *26*, 305701−305707.

(8) Narimanov, E. E.; Kildishev, A. V. Naturally hyperbolic. *Nat. Photonics* **2015**, *9*, 214−216.

(9) Basov, D. N.; Fogler, M. M.; Garcia de Abajo, J. J. Polaritons in van der Waals materials. *Science* **2016**, *354*, aag1992.

(10) Basov, D. N.; Asenjo-Garcia, A.; Schuck, P. J.; Zhu, X.; Rubio, A. Polariton panorama. *Nanophotonics* **2020**, *10*, 549.

(11) Basov, D. N.; Timusk, T. Electrodynamics of high-T_c superconductors. *Rev. Mod. Phys.* **2005**, *77*, 721−779.

(12) Smolyaninova, V. N.; Yost, B.; Zander, K.; Osofsky, M. S.; Kim, H.; Saha, S.; Greene, R. L.; Smolyaninov, I. I. Experimental demonstration of superconducting critical temperature increase in electromagnetic metamaterials. *Sci. Rep.* **2015**, *4*, 7321.

(13) Buisson, O.; Xavier, P.; Richard, J. Observation of propagating plasma modes in a thin superconducting film. *Phys. Rev. Lett.* **1994**, *73*, 3153−3156.

(14) Yu, Y.; Ma, L.; Cai, P.; Zhong, R.; Ye, C.; Shen, J.; Gu, G. D.; Chen, X. H.; Zhang, Y. High-temperature superconductivity in monolayer $Bi_2Sr_2CaCu_2O_{8+\delta}$. *Nature* **2019**, *575*, 156−163.

(15) Hugall, J. T.; Singh, A.; van Hulst, N. F. Plasmonic cavity coupling. *ACS Photonics* **2018**, *5* (1), 43−53.

(16) Kuzmenko, A. B. Kramers−Kronig constrained variational analysis of optical spectra. *Rev. Sci. Instrum.* **2005**, *76*, 083108−083116.

(17) Tu, J. J.; Homes, C. C.; Gu, G. D.; Basov, D. N.; Strongin, M. Optical studies of charge dynamics in optimally doped $Bi_2Sr_2CaCu_2O_{8+\delta}$. *Phys. Rev. B* **2002**, *66*, 144514−144518.

(18) Tajima, S.; Gu, G. D.; Miyamoto, S.; Odagawa, A.; Koshizuka, N. Optical evidence for strong anisotropy in the normal and superconducting states in $Bi_2Sr_2CaCu_2O_{8+z}$. *Phys. Rev. B* **1993**, *48*, 16164−16167.

(19) Shibata, H.; Matsuda, A. Josephson plasma frequencies in overdoped $Bi_2Sr_2CaCu_2O_{8+d}$. *Phys. Rev. B* **1999**, *59*, 11672−11674.
(20) Shibata, H. Optical study of the Josephson plasma in high-T_c superconductors. *Physica C* **2002**, *367*, 360−364.
(21) Sun, Z.; Fogler, M. M.; Basov, D. N.; Millis, A. J. Collective modes and terahertz near-field response of superconductors. *Phys. Rev. Res.* **2020**, *2*, 023413−023432.
(22) Gabriele, F.; Udina, M.; Benfatto, L. Non-linear Terahertz Driving of Plasma Waves in Layered Cuprates. 2020, 2006.02296. Arxiv. https://arxiv.org/pdf/2006.02296.pdf (accessed September 7, 2020).
(23) Nicoletti, D.; Cavalleri, A. Nonlinear light−matter interaction at terahertz frequencies. *Adv. Opt. Photonics* **2016**, *8*, 401−464.
(24) Pohl, D. W.; Denk, W.; Lanz, M. Optical stethoscopy: Image recording with resolution $\lambda/20$. *Appl. Phys. Lett.* **1984**, *44*, 651−653.
(25) Denk, W.; Pohl, D. W. Near-field optics: Microscopy with nanometer-size fields. *J. Vac. Sci. Technol., B: Microelectron. Process. Phenom.* **1991**, *9*, 510−513.
(26) Amarie, S.; Ganz, T.; Keilmann, F. Mid-infrared near-field spectroscopy. *Opt. Express* **2009**, *17*, 21794−21801.
(27) Atkin, J. M.; Berweger, S.; Jones, A. C.; Raschke, M. B. Nano-optical imaging and spectroscopy of order, phases, and domains in complex solids. *Adv. Phys.* **2012**, *61*, 745−842.
(28) Chen, X.; Hu, D.; Mescall, R.; You, G.; Basov, D. N.; Dai, Q.; Liu, M. Modern scattering-type scanning near-field optical microscopy for advanced material research. *Adv. Mater.* **2019**, *31*, 1804774.
(29) Ni, G. X.; McLeod, A. S.; Sun, Z.; Wang, L.; Xiong, L.; Post, K. W.; Sunku, S. S.; Jiang, B.-Y.; Hone, J.; Dean, C. R.; Fogler, M. M.; Basov, D. N. Fundamental limits to graphene plasmonics. *Nature* **2018**, *557*, 530−533.
(30) Dai, S.; Ma, Q.; Andersen, T.; McLeod, A. S.; Fei, Z.; Liu, M. K.; Wagner, M.; Watanabe, K.; Taniguchi, T.; Thiemens, M.; Keilmann, F.; Jarillo-Herrero, P.; Fogler, M. M.; Basov, D. N. Subdiffractional focusing and guiding of polaritonic rays in a natural hyperbolic material. *Nat. Commun.* **2015**, *6*, 1−7.
(31) Li, P.; Lewin, M.; Kretinin, A. V.; Caldwell, J. D.; Novoselov, K. S.; Taniguchi, T.; Watanabe, K.; Gaussmann, F.; Taubner, T. Hyperbolic phonon-polaritons in boron nitride for near-field optical imaging and focusing. *Nat. Commun.* **2015**, *6*, 1−9.
(32) Pons-Valencia, P.; Alfaro-Mozaz, F. J.; Wiecha, M. M.; Biolek, V.; Dolado, I.; Velez, S.; Li, P.; Alonso-Gonzalez, P.; Casanova, F.; Hueso, L. E.; Martin-Moreno, L.; Hillenbrand, R.; Nikitin, A. Y. Launching of hyperbolic phonon-polaritons in h-BN slabs by resonant metal plasmonic antennas. *Nat. Commun.* **2019**, *10*, 1−8.
(33) Woessner, A.; Lundeberg, M. B.; Gao, Y.; Principi, A.; Alonso-Gonazalez, P.; Carrega, M.; Watanabe, K.; Taniguchi, K.; Vignale, G.; Polini, M.; Hone, J.; Hillenbrand, R.; Koppens, F. H. L. Highly confined low-loss plasmons in graphene−boron nitride heterostructures. *Nat. Mater.* **2015**, *14*, 421−425.
(34) Ni, G. X.; Wang, L.; Goldflam, M. D.; Wagner, M.; Fei, Z.; McLeod, A. S.; Liu, M. K.; Keilmann, F.; Ozyilmaz, B.; Castro Neto, A. H.; Hone, J.; Fogler, M. M.; Basov, D. N. Ultrafast optical switching of infrared plasmon polaritons in high-mobility graphene. *Nat. Photonics* **2016**, *10*, 244−247.
(35) Lundeberg, M. B.; Gao, Y.; Asgari, R.; Tan, C.; Van Duppen, B.; Autore, M.; Alonso-Gonzalez, P.; Woessner, A.; Watanabe, K.; Taniguchi, T.; Hillenbrand, R.; Hone, J.; Polini, M.; Koppens, F. H. L. Tuning quantum nonlocal effects in graphene plasmonics. *Science* **2017**, *357*, 187−191.
(36) Brar, V. W.; Jang, M. S.; Sherrott, M.; Kim, S.; Lopez, J. J.; Kim, L. B.; Choi, M.; Atwater, H. Hybrid surface-phonon-plasmon polariton modes in graphene/monolayer h-BN heterostructures. *Nano Lett.* **2014**, *14*, 3876−3880.
(37) Dai, S.; Ma, Q.; Liu, M. K.; Andersen, T.; Fei, Z.; Goldflam, M. D.; Wagner, M.; Watanabe, K.; Taniguchi, T.; Thiemens, M.; Keilmann, F.; Janssen, G. C. A. M.; Zhu, S-E.; Jarillo-Herrero, P.; Fogler, M. M.; Basov, D. N. Graphene on hexagonal boron nitride as a tunable hyperbolic metamaterial. *Nat. Nanotechnol.* **2015**, *10*, 682−686.
(38) Caldwell, J. D.; Aharonovich, I.; Cassabois, G.; Edgar, J. H.; Gil, B.; Basov, D. N. Photonics with hexagonal boron nitride. *Nat. Rev. Mater.* **2019**, *4*, 552−567.
(39) Zhan, T.; Shi, X.; Dai, Y.; Liu, X.; Zi, J. Transfer matrix method for optics ingraphene layers. *J. Phys.: Condens. Matter* **2013**, *25*, 215301−215310.
(40) Fei, Z.; Rodin, A. S.; Andreev, G. O.; Bao, W.; McLeod, A. S.; Wagner, M.; Zhang, L. M.; Zhao, Z.; Thiemens, M.; Dominguez, G.; Fogler, M. M.; Castro Neto, A. H.; Lau, C. N.; Keilmann, F.; Basov, D. N. Gate-tuning of graphene plasmons revealed by infrared nano-imaging. *Nature* **2012**, *487*, 82−85.
(41) Caldwell, J. D.; Kretinin, A. V.; Chen, Y.; Giannini, V.; Fogler, M. M.; Francescato, Y.; Ellis, C. T.; Tischler, J. G.; Woods, C. R.; Giles, A. J.; Hong, M.; Watanabe, K.; Taniguchi, T.; Maier, S. A.; Novoselov, K. S. Sub-diffractional volume-confined polaritons in the natural hyperbolic material hexagonal boron nitride. *Nat. Commun.* **2014**, *5*, 1−9.
(42) Yampol'Skii, V. A.; Savel'ev, S.; Rakhmanov, A. L.; Nori, F. Nonlinear electrodynamics in layered superconductors. *Phys. Rev. B* **2008**, *78* (2), 024511−024519.
(43) Ooi, K. J. A.; Tan, D. T. H. Nonlinear graphene plasmonics. *Proc. R. Soc. A* **2017**, *473* (2206), 20170433.
(44) Gruninger, M.; van der Marel, D.; Tsvetkov, A. A.; Erb, A. Observation of out-of-phase bilayer plasmons in $YBa_2Cu_3O_{7-\delta}$. *Phys. Rev. Lett.* **2000**, *84* (7), 1575−1578.
(45) van der Marel, D.; Tsvetkov, A.; Gruninger, M.; Dulic, D.; Molegraaf, H. J. A. C-axis optical properties of high T_c cuprates. *Physica C* **2000**, *341-348*, 1531.
(46) Tajima, S.; Zelezny, V.; Motohashi, T.; Shimoyama, J.; Kishio, K.; Munzar, D. Optical response of the Josephson coupled CuO_2-layers in high-T_c superconductors. *Physica C* **2001**, *362*, 86−91.
(47) Zelezny, V.; Tajima, S.; Munzar, D.; Motohashi, T.; Shimoyama, J.; Kishio, K. Anomalies in the infrared spectra of underdoped $Bi_2Sr_2CaCu_2O_z$ as evidence for the intrabilayer Josephson effect. *Phys. Rev. B* **2001**, *63* (6), 060502−060505.
(48) Adam, A. J. L. Review of near-field terahertz measurement methods and their applications. *J. Infrared, Millimeter, Terahertz Waves* **2011**, *32*, 976−1019.
(49) Rizzo, D. J.; Jessen, B. S.; Sun, Z.; Ruta, F. L.; Zhang, J.; Yan, J.-Q.; Xian, L.; McLeod, A. S.; Berkowitz, M. E.; Watanabe, K.; Taniguchi, T.; Nagler, S. E.; Mandrus, D. G.; Rubio, A.; Fogler, M. M.; Millis, A. J.; Hone, J. C.; Dean, C. R.; Basov, D. N. Charge-Transfer Plasmon Polaritons at Graphene/α-RuCl $_3$ Interfaces. *Nano Lett.* **2020**, *20*, 8438−8445.
(50) Efetov, D. K.; Wang, L.; Handschin, C.; Efetov, K. B.; Shuang, J.; Cava, R.; Taniguchi, T.; Watanabe, K.; Hone, J.; Dean, C. R.; Kim, P. Specular interband Andreev reflections at van der Waals interfaces between graphene and $NbSe_2$. *Nat. Phys.* **2016**, *12*, 328−332.
(51) Di Bernardo, A.; Millo, O.; Barbone, M.; Alpern, H.; Kalcheim, Y.; Sassi, U.; Ott, A. K.; De Fazio, D.; Yoon, D.; Amado, M.; Ferrari, A. C.; Linder, J.; Robinson, J. W. A. *p*-wave triggered superconductivity in single-layer graphene on an electron-doped oxide superconductor. *Nat. Commun.* **2017**, *8*, 1−9.
(52) Costa, A. T.; Goncalves, P. A. D.; Koppens, F. H. L.; Basov, D. N.; Asger Mortensen, N.; Peres, N. M. R. Harnessing Ultra-confined Graphene Plasmons to Probe the Electrodynamics of Superconductors; 2020. 2006.00748. Arxiv. https://arxiv.org/pdf/2006.00748.pdf (accessed September 7, 2020).
(53) Pizzocchero, F.; Gammelgaard, L.; Jessen, B. S.; Caridad, J. M.; Wang, L.; Hone, J.; Bøggild, P.; Booth, T. J. The hot pick-up technique for batch assembly of van der Waals heterostructures. *Nat. Commun.* **2016**, *7*, 1−10.
(54) Purdie, D. G.; Pugno, N. M.; Taniguchi, T.; Watanabe, K.; Ferrari, A. C.; Lombardo, A. Cleaning interfaces in layered materials heterostructures. *Nat. Commun.* **2018**, *9*, 1−12.
(55) Alonso-Gonzalez, P.; Nikitin, A. Y.; Gao, Y. W.; Woessner, A.; Lundeberg, M.; Principi, A.; Forcellini, N.; Yan, W.; Velez, S.; Huber, A. J.; Watanabe, K.; Taniguchi, T.; Casanova, F.; Hueso, L. E.; Polini, M.; Hone, J.; Koppens, F. H. L.; Hillenbrand, R. Acoustic terahertz

graphene plasmons revealed by photocurrent nanoscopy. *Nat. Nanotechnol.* **2017**, *12*, 31−35.
(56) Yang, H. U.; Hebestreit, E.; Josberger, E. E.; Raschke, M. B. A cryogenic scattering-type scanning near-field optical microscope. *Rev. Sci. Instrum.* **2013**, *84*, 023701−023705.
(57) Sentef, M. A.; Ruggenthaler, M.; Rubio, A. Cavity quantum-electrodynamical polaritonically enhanced electron-phonon coupling and its influence on superconductivity. *Sci. Adv.* **2018**, *4* (11), eaau6969.
(58) Ashida, Y.; Imamoglu, A.; Faist, J.; Jaksch, D.; Cavalleri, A.; Demler, E. Quantum Electrodynamic Control of Matter: Cavity-Enhanced Ferroelectric Phase Transition. *Phys. Rev. X* **2020**, *10*, 041027−041059.

https://dx.doi.org/10.1021/acs.nanolett.0c03684
Nano Lett. 2021, 21, 308−316